Journal of Science: Advanced Materials and Devices 5 (2020) 256–262

Contents lists available at ScienceDirect

Journal of Science: Advanced Materials and Devices

journal homepage: www.elsevier.com/locate/jsamd

Original Article

Oxide charge evolution under crystallization of amorphous Li–Nb–O films

M. Sumets [a, *], V. Ievlev [a, b], E. Belonogov [c], V. Dybov [c], D. Serikov [c], G. Kotov [d], A. Turygin [e]

[a] Voronezh State University, Universitetskaya Square, 1, 394000, Voronezh, Russia
[b] Lomonosov Moscow State University, Leninskie Gory, Moscow, 119991, Russia
[c] Voronezh State Technical University, Prosp. Moskovskij, 14, Voronezh, Russia
[d] Voronezh State University of Engineering Technologies, Revolution Av., 19, 394036, Voronezh, Russia
[e] School of Natural Sciences and Mathematics, Ural Federal University, 51 Lenin av., 620000 Ekaterinburg, Russia

ARTICLE INFO

Article history:
Received 30 September 2019
Received in revised form
17 February 2020
Accepted 23 February 2020
Available online 5 March 2020

Keywords:
$LiNbO_3$
Crystallization
Magnetron sputtering
Oxide charge
Annealing

ABSTRACT

Li–Nb–O amorphous films were deposited onto Si substrates by the radio-frequency magnetron sputtering method in an Ar environment and an Ar(60%)+O_2(40%) gas mixture. A positive effective fixed oxide charge Q_{eff} having negative, -Q_{eff}, and positive, +Q_{eff}, components, exists in the as-grown heterostructures. -Q_{eff} is located near the substrate/film interface, whereas + Q_{eff} is determined by a deficit of Li and O (vacancies) in the bulk of Li–Nb–O films. As-grown films crystallized under thermal annealing (TA) at temperatures up to 600 °C and revealed the formation of polycrystalline $LiNbO_3$. TA at about 520 °C resulted in the formation of the second phase $LiNb_3O_8$, increasing + Q_{eff}, and compensating -Q_{eff} entirely. The dielectric constants of the as-grown films exhibit two peaks at the annealing temperatures of 450 °C and 550 °C, which are attributed to the total crystallization and recrystallization of the LN films under TA, respectively.

1. Introduction

Ferroelectric oxides in a thin-film form are essential components in a variety of applications. They have been used in various sensor and actuator designs, in optoelectronics and in rf devices for tunable microwave circuits. Moreover, thin ferroelectric films have contributed to the prospects for multifunctional optical integrated circuits. Lithium niobate ($LiNbO_3$, in short LN) is one of the most promising ferroelectric materials due to its high Curie temperature (T_c = 1210 °C), large bandgap (E_g = 3.7eV) and, favorable piezoelectric and electro-optical coefficients. Currently, $LiNbO_3$ is the golden standard for electro-optical material in fiber-optic transmission systems [1]. The integration ability of LN into the existing technology is especially important in view of the creation of various devices such as non-volatile memory units, optical modulators, microring optical resonators, acoustic delay lines, etc [2]. However, the practical application requires the formation of LN-based heterostructures (like Si-LN) with specific properties. Specifically, the non-volatile ferroelectric random access memories are based on the polarization reversal by an external applied electric field of metal-ferroelectric-metal capacitors or metal-ferroelectric-semiconductor heterostructures. Thus, one of the objectives is to find a ferroelectric material demonstrating little or no degradation of the switchable ferroelectric polarization [3]. This requirement, as well as other features like optical loss, depends on both the LN film properties and the characteristics of the LN film/substrate interface. Various methods have successfully been used for deposition of LN films: chemical vapor deposition (CVD) [4], liquid phase epitaxy [5] and pulsed laser deposition [6]. Radio-frequency magnetron sputtering (RFMS) is among the effective processes for growing films of complex oxides like LN, while preserving the initial elemental composition [7]. It is generally accepted that the thin film properties are very sensitive to the deposition method. For example, it was demonstrated that these properties are influenced greatly by the RFMS conditions [8–10]. Besides, thermal annealing (TA), being an effective method of improving properties of as-grown polycrystalline films, changes their characteristics dramatically [8,11,12]. An alternative approach to fabricate highly oriented films is the formation of amorphous films followed by crystallization through TA.

* Corresponding author.
E-mail address: maxsumets@gmail.com (M. Sumets).
Peer review under responsibility of Vietnam National University, Hanoi.

https://doi.org/10.1016/j.jsamd.2020.02.006

Table 1
Fabrication regimes for the studied samples.

Sample #	Reactive gas environment	Reactive gas pressure, Pa	Magnetron power, W	Substrate type	Substrate temperature	Film thickness d, nm	Annealing duration and atmosphere
S1	Ar	1.5×10^{-1}	100	Si, n-type, $\rho = 4.5$ Ω cm	550 °C	3000	–
S2						300	–
S3						100	–
S4			50		unheated	300	60min in air
S5						100	
S6	Ar(60%)+O_2(40%)					100	

Some applications such as non-volatile memory units and field-effect transistors (FeFET), require the formation of thin oxide films with a high dielectric constant (ε = 200–2000), a low current leakage [13] and a high breakdown voltage (E = 300-10^3 kV/cm [14]). These parameters are very sensitive to the composition and point defects (Li and O) [15], and to the charge localization centers at the film surface [16]. Besides, the charged defects in LN influence not only the electrical but also the optical ferroelectric properties [8,15,17–19]. Specifically, if a depletion layer is connected in series to a film, the high dielectric constant of the gate materials results in a depolarization field [20]. Thus, it is very hard to achieve long retention times of the stored polarization state in scaled-down FeFET devices. Besides, some researchers, working in the cutting edge of ferroelectric memory design, revealed that the charges, existing in a ferroelectric material, depress the polarization reversal, which is vital for its effective memory application [20]. On the other hand, other investigators exploited oxygen vacancies to fabricate memristive systems based on the ferroelectric diodes employing LN [21]. They reported about I–V characteristics of the Pt/LN/Pt metal-ferroelectric-metal capacitor, which demonstrates memristive behavior. Oxygen vacancies, accumulated at the bottom Pt/LN interface, play a crucial role in this device by "memorizing" the switched state through electron trapping. Another research group reported about rectifying filamentary resistive switching after forming of LN films [22]. This phenomenon is interpreted by a model that the local filament does not penetrate throughout the $LiNbO_3$ thin film, resulting in asymmetric contact barriers at the two interfaces. The reason is that oxygen vacancies with high concentrations are generated during TA in an Argon environment for the formation of conductive filaments. Remarkably, the filaments composed by oxygen vacancies do not penetrate throughout the $LiNbO_3$ film. Authors pointed up that it can be potentially applicable in high-density memories, requiring uniform performance among different cells.

Despite the important role being played by the oxide charge in ferroelectric memories the origin and distribution of this charge in LN-based heterostructures during the crystallization of LN films are not clear yet.

The present work is aimed to investigate how the oxide charge evolves during the crystallization of amorphous Li–Nb–O films deposited onto Si substrates.

2. Experimental

The studied samples were fabricated by depositing the Li–Nb–O system onto silicon wafers (Si(001), n-type conductivity, $\rho = 4.5$ Ohm·cm) by RFMS of the $LiNbO_3$ targets.[1] In this work, we used the sputtering conditions given in Table 1. Silicon wafers were cleaned by ion etching in an Ar plasma (2 min) before the RFMS process.

[1] The targets were fabricated in the Institute of Chemistry and Technology of Rare Elements and Mineral Raw Materials of the Russian Academy of Science (Apatity).

The structure and composition of the studied films were investigated by X-ray diffraction method (XRD, ARL X'TRA Thermo Techno), high-resolution transmission electron microscopy (TEM, FEI Titan-300), and scanning electron microscopy (SEM, FEI HELIOS Nanolab). A powder diffractometer (with a Cu Kα source operated at 40 kV and 35 mA) scanned in the parallel beam geometry (optical scheme: a parabolic mirror – a thin film collimator) in the θ-θ regime. The energy-dispersive X-ray microanalysis (EDAM for SEM and transmission (STEM) electron microscopy) was used to obtain the concentration profile of elements as a function of depth. The STEM images were obtained by registering the low- and high-angle scattered electrons.

The spatial distribution of the surface potential was visualized using the scanning probe microscope Asylum MFP-3D (Asylum Research, Oxford Instruments, UK) in the closed-loop two-pass Kelvin Probe Force Microscopy (KPFM) mode. A 0.5 V_{AC} voltage is applied to the tip and a distance between tip and surface of 200 nm at the second pass. Commercial AFM probes NSC18 with titanium–platinum-conductive coating (MikroMash, Estonia) with a curvature radius of R_{tip} = 35 nm, a resonance frequency of f_{res} = 70 kHz, and a spring constant of k = 3.5 N/m were used. The measurements were conducted in a dry atmosphere with a relative humidity of less than 5% provided by a constant flow of nitrogen through the microscope chamber.

The electrical properties of the studied samples were investigated with the use of high frequency (f = 10^5 Hz) capacitance–voltage (C–V) characteristics and current–voltage (I–V) characteristics at a temperature of T = 300K. The top contacts ($S = 8 \cdot 10^{-7}$ m^2) for electrical measurements were created by thermal evaporation and condensation of Al in vacuum. The bottom contacts were created by spreading the In/Ga eutectic alloy on the Si substrate ensuring the formation of Ohmic contacts.

3. Results and discussion

Fig. 1 shows the structure and composition of both as-grown Li–Nb–O films and the films after TA deposited onto Si substrates under regimes, corresponding to the sample S4 from Table 1.

As follows from Fig. 1(a–c), thin Li–Nb–O films are morphologically non-homogeneous and have an amorphous structure. The inhomogeneities consist of anisotropic aggregates which are comparable in size with the film (the lateral dimension ranges from 15 to 50 nm, the vertical dimension is 250 nm). The analysis of STEM images suggests that the aggregate boundaries have a higher amount of light elements (oxygen and lithium) compared to the bulk.

The EDAM results reveal the gradient in elemental composition (see Fig. 1(g–h)). The Nb/O ratio changes from 0.33 at the film/substrate interface to 0.5 at the film surface. The periodic change in the concentration of elements corresponds to the separate film layers with a thickness of 15 nm, which correlates with the amorphous aggregates dimension.

The annealed films demonstrate a crystalline structure with a morphological inhomogeneity (the dispersed crystallites 50 nm in

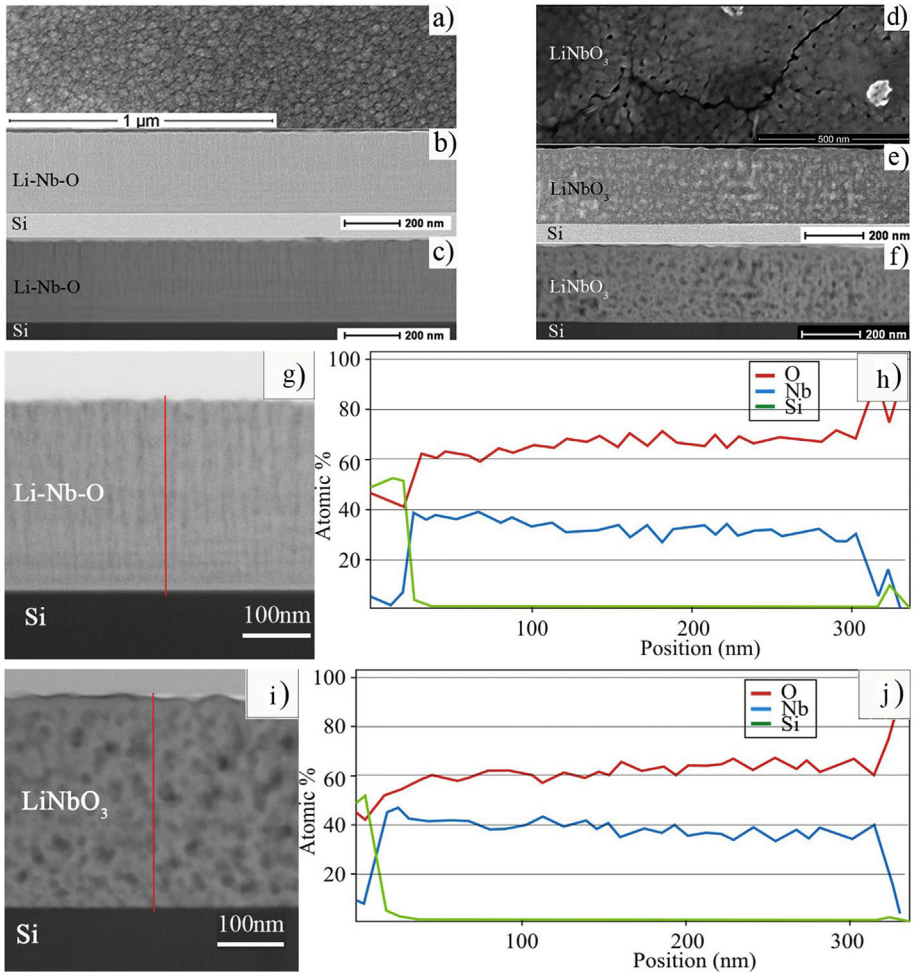

Fig. 1. The structure and composition of both as-grown Li–Nb–O films and the films after TA deposited under regimes, corresponding to sample S4 from Table 1. a–f: the SEM images of a surface (a, d) and the cross-sectional bright- (b, e) and dark-field (c, f) TEM images of both as-grown Li–Nb–O films (a,b,c) and after TA (d,e,f). g–j: the cross-sectional dark-field TEM image and distribution of elements in as-grown Li–Nb–O films (g,h) and after TA (i,j).

size). As follows from the bright- and dark-field TEM images (see Fig. 1 (e) and (f)), the elemental composition in the adjacent crystallites differs greatly. The Nb/O ratio changes from 0.6 at the Si/LN interface to 0.8 at the LN film surface (see Fig. 1(i–j)).

As reported in our previous works [10,23], the thermal annealing reduces the positive effective charge Q_{eff}, which existed in as-grown Si-LN heterostructures with the polycrystalline LN films. Moreover, at annealing the Si-LN heterostructures fabricated by the RFMS method in an Ar + O_2 environment Q_{eff} changed its sign from positive to negative [23]. Currently, it is unclear whether Q_{eff} is located: in the bulk of the LN films or at the Si/LN interface. In our previous works, we studied "thick" LN film-based heterostructures and Q_{eff} was always found to be positive [10,24]. Besides, we reported that TA at a temperature of 650 °C reduces Q_{eff}. Moreover, Si-LN heterostructures fabricated by RFMS technique in an Ar + O_2 gas mixture and annealed at a temperature of 650 °C for 1 h manifested the negative Q_{eff} [23,24]. In this work, we studied the evolution of Q_{eff} in as-grown heterostructures annealed at various temperatures.

The typical C–V characteristics of Si-LN heterostructures grown in an Ar environment with LN layers of different thicknesses were analogous to those for the metal-oxide-semiconductor (MOS) structures (see Fig. 2) [25].

All curves shown in Fig. 2 are shifted along the horizontal axis relative to the corresponding theoretical C–V characteristics. According to the standard theory of MOS heterostructures [25], it is due to the effective oxide charge Q_{eff}, existing in the studied

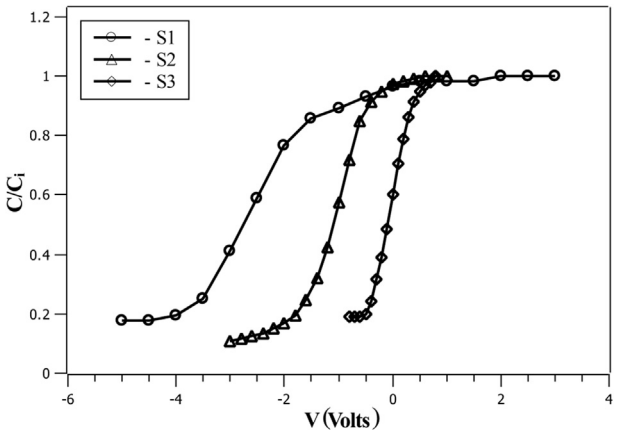

Fig. 2. Typical normalized C–V characteristics of the studied heterostructures.

samples. Fig. 3 shows how Q_{eff} depends on the film thickness in the studied Si-LN heterostructures.

As seen from Fig. 3, the effective oxide charge is negative for the "thin" (d < 200 nm) LN films and positive for the "thick" (d > 200 nm) films and increases with thickness. According to literature data, the LN film thickness affects its electrical properties greatly. Specifically, authors of reference [26] reported that "thick" polycrystalline LN films with a small grain size demonstrate a high concentration of oxygen defects and defect dipole complexes, located near the grain boundaries. These defects, being positively charged, give rise to + Q_{eff} for the thick LN films in our case. Fig. 4 demonstrates typical C–V characteristics of the studied samples.

Fig. 5 shows the effective oxide charge Q_{eff} as a function of annealing temperature T_a for the studied samples, derived from their C–V characteristics at different T_a.

Additionally, for confirming the correct interpretation of Q_{eff} derived from C–V measurements we conducted KPFM measurements for sample S5. The obtained results are given in Fig. 6. The KPFM measurements of the investigated sample demonstrate a nearly uniform surface potential of about 900 mV with a local decrease of up to 850 mV which can be associated with the inclusions of a secondary phase. Besides, the KPFM scanning was carried out at various distances *h* from the sample.

The average surface potential as a function of a tip-surface distance obtained by the KPFM technique for the as-grown sample S5 is shown in Fig. 7.

Taking into account the linear dependence of $V_{surf}(h)$ (see Fig. 7) and assuming an uniform charge distribution at the sample surface, we estimated the Q_{eff} value through the following expression for the electric field of a charged surface:

$$-\frac{dV}{dh} = \frac{Q_{eff}}{2\varepsilon\varepsilon_0} \quad (1)$$

here ε_0 is dielectric permittivity of free space. The obtained values for various T_A are represented by the S5 (KPFM) curve in Fig. 5 and correlate with those derived from C–V characteristics (see Fig. 3).

It follows from Fig. 5 that the as-grown heterostructures (fabricated in an Ar environment) with the "thin" amorphous Li–Nb–O films contain a negative Q_{eff} (samples S5 and S6), whereas the "thick" film-based samples demonstrate a positive effective charge. This result agrees with data for the polycrystalline films (see Fig. 3). Further TA changes the Q_{eff} values. It is worth noting that the value of Q_{eff} varies oppositely for heterostructures with the "thick" and "thin" films: when the value of $|+Q_{eff}|$ increases, the value of $|-Q_{eff}|$ decreases, and vice versa (see samples S4 and S5 in Fig. 5). This can be explained by assuming that the effective charge has two components: the negative charge ($-Q_{eff}$, located near the Si/LN interface or at the film surface) and the positive charge ($+Q_{eff}$, distributed in the bulk of LN films). Analysis of various models reveals that the charged antisite defects like Nb_{Li}^{4+} or oxygen vacancies are the most plausible origins of the positive oxide charge [18].

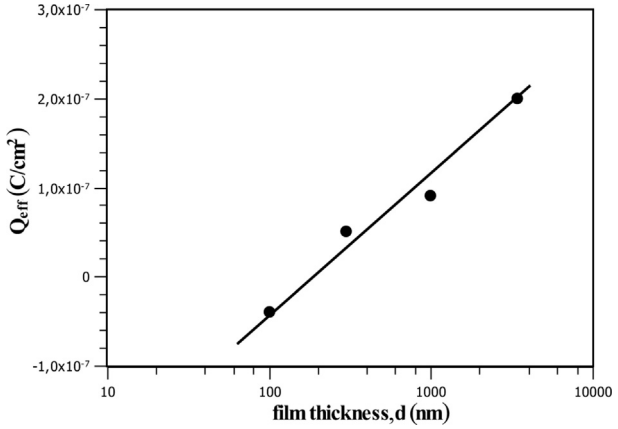

Fig. 3. The effective oxide charge as a function of the film thickness in Si-LN heterostructures.

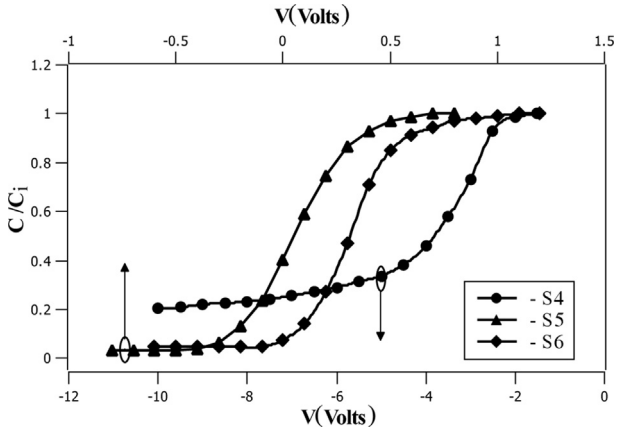

Fig. 4. Normalized C–V characteristics of as-grown heterostructures annealed at T_a = 400 °C. C_i is the geometry capacitance of an LN layer.

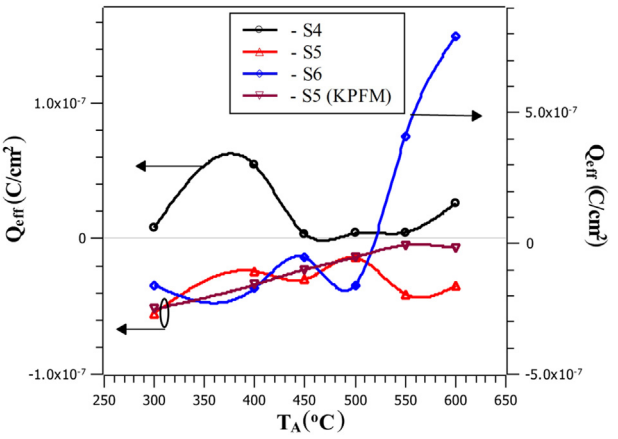

Fig. 5. The effective oxide charge as a function of the annealing temperature for the studied heterostructures.

Li and O vacancies can be created in the deposited $LiNbO_3$ thin film due to its volatile nature and out-diffusion from the film according to the following possible reactions [25]:

$$\begin{aligned} LiNbO_3 &\rightarrow Li_2O + 2\,V_{Li}^{-} + VO_2^{+} \\ LiNbO_3 &\rightarrow 3\,Li_2O + 4\,V_{Li}^{-} + Nb_{Li}^{4+} \end{aligned} \quad (2)$$

On the other hand, according to the model proposed in [18], the structural defects can be redistributed as follows:

$$3O_O + 2\,V_{Li}^{-} + Nb_{Nb} \leftrightarrow \frac{3}{2}O_2 + Nb_{Li}^{4+} + 6e^{-} \quad (3)$$

Therefore, the formation of the antisite defects Nb_{Li}^{4+}, as well as the oxygen vacancies (VO_2^{+}) distributed in the bulk of a film, are likely to be the origin of the positive charge in the as-grown Li–Nb–O films.

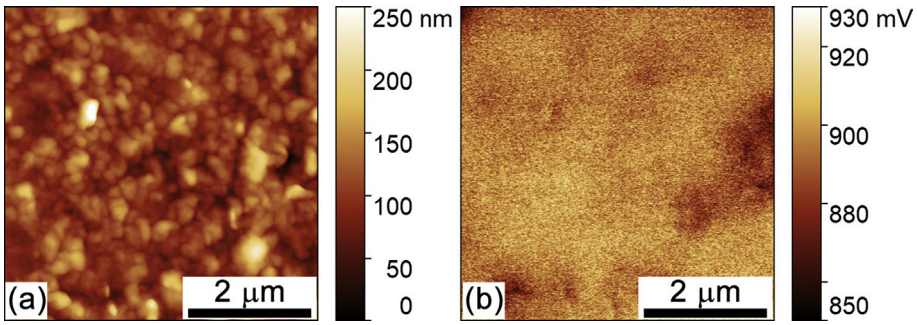

Fig. 6. The surface topography (a) and surface potential (b) of sample S5 obtained by the KPFM method.

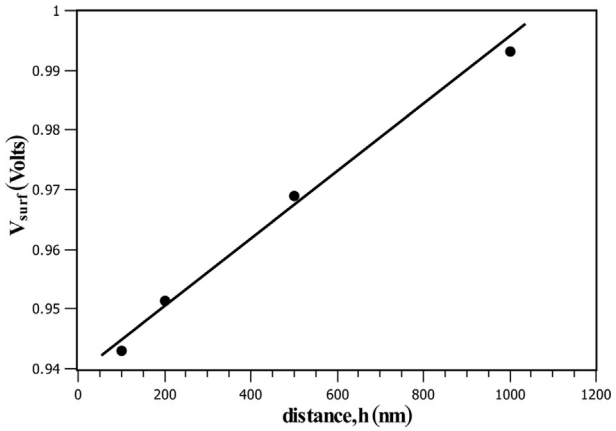

Fig. 7. Average surface potential as a function of a distance from the scanned surface for sample S5.

If oxygen is present in the reactive chamber, it fills the existing oxygen vacancies, and the positive charge declines. Another explanation can be based on the formation of the $V_{Li}^{-} - {}^{1}/_{2}O_2$ complex with the formation of a negative charge, compensating partially the positive one. The following reaction describes the possible charge transfer, occurring in case oxygen resides in the nearest position with a lithium vacancy [8]:

$$V_{Li}^{-} + \frac{1}{2} O_2 \Rightarrow V_{Li}^{0} + \frac{1}{2} O_2^{-} \quad (4)$$

Consequently, in Li–Nb–O films grown in an Ar + O_2 gas mixture, the positive charge has to be lower which agrees with our results presented in Fig. 5.

It was established [26] that for films annealed in an oxygen atmosphere, the concentration of lithium decreases, slightly affecting the decrease of lithium and oxygen vacancies and resulting in the positive charge in our case. Based on these models, oxygen diffusing in a film during TA decreases the concentration of vacancies and consequently, the $+Q_{eff}$ value. Apparently, in heterostructures with "thin" LN films $-Q_{eff}$ dominates which is associated with structural defects near the Si/LN interface. By contrast, in the "thick" LN films + Q_{eff} can be attributed to oxygen vacancies or Nb_{Li}^{4+} defects and it prevails over the interface-based negative charge. As it was mentioned above, amorphous films deposited onto Si substrates, are crystallized in LN with a significant oxygen deficit under TA. This fact is supported by our results on the elemental composition (see Fig. 1(i–j)). Thermal annealing in air decreases the oxygen deficit in the bulk thick Li–Nb–O films greatly, whereas the change in the interface-based charge does not contribute to the net charge evolution. A negative component of the effective charge in the "thin" films-based heterostructures is higher than the positive one and the change in $+Q_{eff}$ is detected as an opposite variation in $-Q_{eff}$ (which is the net charge). As follows from our recent work, TA results in the crystallization of amorphous Li–Nb–O films with the formation of polycrystalline LN films at the temperature of 470 °C [27]. This temperature nearly corresponds to the minimum net charge in Si-LN heterostructures (see Fig. 8 for samples S4 and S5).

TA does not change the oxygen content considerably in the crystallized thick LN films. Thus, the change in Q_{eff} after TA of as-grown films at temperatures over 470 °C can be explained by redistribution of oxygen atoms, out from bulk to grain boundaries. The redistribution degree is determined by the change in specific concentration of grain boundaries, formed in the film's crystallization process. The results, reported in work [28], support this mechanism. The authors of this work studied the TA effect on the composition and structure of the topmost layers of $LiNbO_3$ single crystals through co-axial impact collision ion scattering spectroscopy and X-ray photoelectron spectroscopy. They revealed that due to the desorption of Li_2O, the topmost layers of the crystal at the temperature of 400°C demonstrate a deficit of Li and O (with the formation of corresponding vacancies) which agrees with our results (see Fig. 1(i–j)). However, due to the out-off diffusion of Li and O from the bulk LN, the further annealing at higher temperatures up to 600°C led to decelerate the loss of these elements. This process is reflected by the increase in $+Q_{eff}$ in Fig. 5 at temperatures of $T_A > 550$ °C. Most prominently, this effect is observed for heterostructures, fabricated in an Ar + O_2 reactive gas mixture. In this case, the presence of O_2 in a reactive chamber minimizes the oxygen deficit (positive effective charge) in amorphous as-grown Li–Nb–O films. Thus, $-Q_{eff}$ (located near the Si/LN interface) in thin films is not compensated by $+ Q_{eff}$ and it contributes to the net charge shown in Fig. 5 for sample S6.

TA at temperatures higher than 520 °C leads to the formation of the $LiNb_3O_8$ phase with a lithium deficit [27], promoting the formation of Nb_{Li}^{4+} defects according to equations (2) and (3). In that case, the positive effective charge rises sharply in LN films (see Fig. 5), compensating the $-Q_{eff}$ entirely. This phenomenon can be used for the fabrication of Si-LN heterostructures free from the effective oxide charge with a potential application in non-volatile memory units. Specifically, the charged domain walls which play a key role in the domain wall memories can draw ionic defects such as oxygen vacancies. This process interferes negatively with the clean and, fluent erasure and regeneration of the domain walls [13].

Based on its definition, the effective charge is the sum of the oxide charge Q_{ox} and the interface charge Q_{ss}, associated with the interface states density N_{ss}. This N_{ss} is defined through the density of interface states per unit energy D_{ss} (which can be extracted from the standard C–V analysis [29]) as follows:

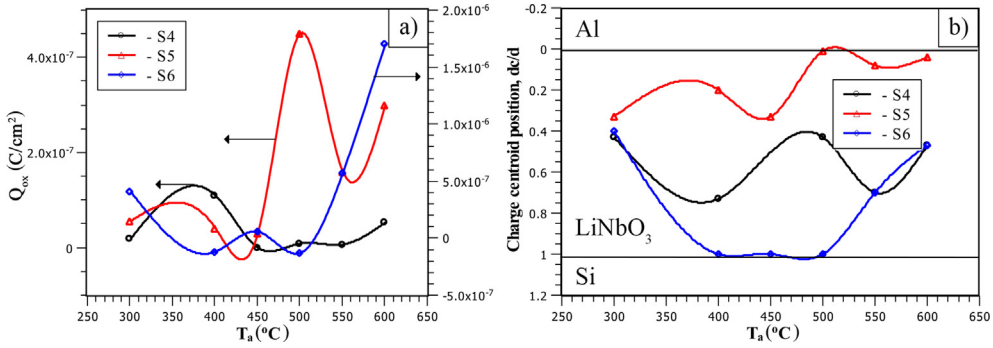

Fig. 8. The oxide charge (a) and its centroid position (b) in the studied Si–$LiNbO_3$–Al heterostructures as a function of the annealing temperature.

$$N_{ss} = \int D_{ss}(E) \cdot f(E)\ \mathrm{d}E \tag{5}$$

here $f(E)$ is the Fermi function.

We calculated the oxide charge as $Q_{ox} = Q_{eff} - Q_{ss}$. The oxide charge centroid position d_c can be determined through the following expression [30]:

$$\Delta V_{FB} = \frac{Q_{ox}}{C_i} \cdot \frac{d_c}{d} \tag{6}$$

here ΔV_{FB} is the shift in the flat band voltage between the experimental and theoretical C–V curves, d is the film thickness.

The oxide charge Q_{ox} and its centroid position as a function of the annealing temperature are shown in Fig. 8.

As seen from Fig. 8, as-grown amorphous Li–Nb–O films contain the positive Q_{ox} with the centroid (the center of mass) located at the center of a film, regardless of the reactive gas environment. In the samples fabricated in an Ar atmosphere, this charge varies similarly to Q_{eff} (see Fig. 5) during the thermal annealing. The charge centroid fluctuates around the center of the film in the "thick" films (sample S4) or approaches the film surface in the "thin" $LiNbO_3$ films (sample S5). As regards the films deposited in an Ar + O_2 gas mixture, Q_{ox} becomes negative and is located near the film/substrate interface (see sample S6 in Fig. 8). This fact supports our guesswork that the negative component of Q_{eff} is located at the Si/$LiNbO_3$ interface.

Fig. 9 demonstrates the dielectric constant ε of the studied heterostructures annealed at various temperatures. As seen from Fig. 9, the ε values of the samples S5 and S6 exhibits two relatively broad peaks at temperatures of about 450 °C and 550 °C.

Similar peaks at 430 °C and 550 °C have been reported by other researchers [31,32] for the amorphous LN films. They confirmed, by XRD analyses and dielectric relaxation study, that the peak at 550 °C corresponds to the re-crystallization of the film, whereas the peak at 430 °C is attributed to the Debye-like relaxation. On the other hand, the bottom of ε between the two peaks observed at 500 °C in Fig. 9, was also reported in [31]. This feature corresponds to the total crystallization of LN films. It has been revealed in our recent work at a temperature of 470 °C. This result agrees with the one given in [31], where it was concluded that a decrease in the value of ε was attributed to the change in the microscopic structure of the films at 490 °C. The values for dielectric constant for single crystal LN are 31 along the a-axis and 78 along the c-axis at 25 °C and 100 kHz [33]. The closest ε to that value for single crystal LN is observed for sample S5. As reported in [34], the dielectric constant of polycrystalline LN films depends greatly on the grain size. For the films with smaller grains, the ε is lower than that for LN films with larger grains.

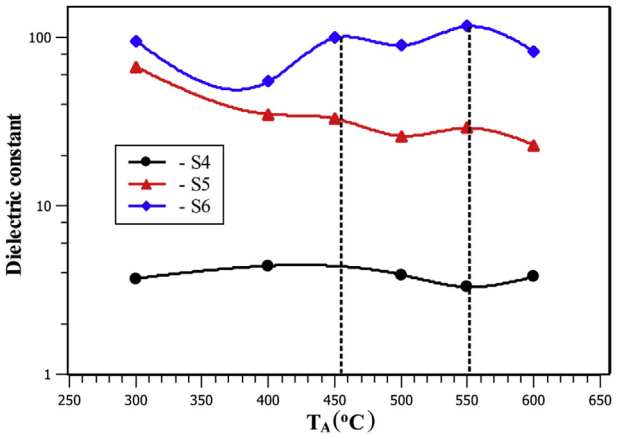

Fig. 9. The dielectric constant as a function of the annealing temperature for the studied samples.

4. Conclusion

The amorphous Li–Nb–O films were deposited onto Si substrates by the RFMS process in an Ar reactive gas environment and an Ar + O_2 gas mixture. All as-grown films manifested the net effective oxide charge having two components: a negative -Q_{eff}, dominating in the "thin" (d < 200 nm) Li–Nb–O films, and a positive + Q_{eff}, prevailing in the "thick" (d > 200 nm) films. -Q_{eff} is attributed to structural defects near the substrate/film interface, whereas + Q_{eff} is determined by a deficit of Li and O (vacancies) in the bulk of Li–Nb–O films. Thermal annealing of as-grown films leads to changes in the vacancies concentration due to the Li_2O desorption, resulting in the change of +Q_{eff}. At the temperature of 470 °C, the as-grown Li–Nb–O films are crystallized with the formation of Si-LN heterostructures having a minimal net oxide charge. Heterostructures, grown in an Ar(60%)+O_2(40%) reactive gas mixture, manifested a lower + Q_{eff} compared to those fabricated in pure Ar. TA at about 520 °C resulted in the formation of the second phase $LiNb_3O_8$, increasing + Q_{eff}, and compensating -Q_{eff} entirely. This process can potentially be used for the fabrication of thin-film Si-LN heterostructures free from the effective oxide charge, which is vital for their practical applications. The dielectric constant of the as-grown films varies non-monotonically during TA and exhibits two peaks at the annealing temperatures of 450 °C and 550 °C. These peaks are attributed to the total crystallization and recrystallization of LN films respectively under TA.

Declaration of Competing Interest

The authors declare no conflict of interest.

Acknowledgments

This research was supported by the Russian Foundation for Basic Research (Grant №18-29-11062 and Grant №18-32-00959). The equipment of the Ural Center for Shared Use “Modern Nanotechnology” of the Ural Federal University was used.

References

[1] A. Bartasyte, S. Margueron, T. Baron, S. Oliveri, P. Boulet, Toward high-quality epitaxial LiNbO3 and LiTaO3 thin films for acoustic and optical applications, Adv. Mater. Interfaces. 4 (2017) 1600998, https://doi.org/10.1002/admi.201600998.

[2] M.P. Sumets, V.A. Dybov, V.M. Ievlev, LiNbO3 films: potential application, synthesis techniques, structure, properties, Inorg. Mater 53 (2017) 1361–1377, https://doi.org/10.1134/S0020168517130015.

[3] N. Setter, D. Damjanovic, L. Eng, G. Fox, S. Gevorgian, S. Hong, A. Kingon, H. Kohlstedt, N.Y. Park, G.B. Stephenson, I. Stolitchnov, A.K. Taganstev, D.V. Taylor, T. Yamada, S. Streiffer, Ferroelectric thin films: review of materials, properties, and applications, J. Appl. Phys. 100 (2006), https://doi.org/10.1063/1.2336999.

[4] B.J. Curtis, H.R. Brunner, The growth of thin films of lithium niobate by chemical vapour de position, Mater. Res. Bull. 10 (1975) 515–520, https://doi.org/10.1016/0025-5408(75)90176-2.

[5] S. Kondo, S. Miyazawa, S. Fushimi, K. Sugii, Liquid-phase-epitaxial growth of single-crystal LiNbO3 thin film, Appl. Phys. Lett. 26 (1975) 489, https://doi.org/10.1063/1.88229.

[6] G. Balestrino, S. Martellucci, P.G. Medaglia, A. Paoletti, G. Petrocelli, A. Tebano, A. Tucciarone, F. Gelli, E. Giorgetti, S. Sottini, L. Tapfer, Epitaxial LiNbO3 thin films grown by pulsed laser deposition for optical waveguides, Appl. Phys. Lett. 78 (2001) 1204–1206, https://doi.org/10.1063/1.1350903.

[7] T.-H. Lee, F.-T. Hwang, C.-T. Lee, H.-Y. Lee, Investigation of LiNbO3 thin films grown on Si substrate using magnetron sputter, Mater. Sci. Eng., B 136 (2007) 92–95, https://doi.org/10.1016/j.mseb.2006.09.001.

[8] A.Z. Simões, M.A. Zaghete, B.D. Stojanovic, A.H. Gonzalez, C.S. Riccardi, M. Cantoni, J.A. Varela, Influence of oxygen atmosphere on crystallization and properties of LiNbO3 thin films, J. Eur. Ceram. Soc. 24 (2004) 1607–1613, https://doi.org/10.1016/S0955-2219(03)00453-9.

[9] X. Wang, Z. Ye, G. Li, B. Zhao, Influence of substrate temperature on the growth and optical waveguide properties of oriented LiNbO 3 thin films, J. Cryst. Growth 306 (2007) 62–67, https://doi.org/10.1016/j.jcrysgro.2007.05.016.

[10] M. Sumets, V. Ievlev, A. Kostyuchenko, V. Kuz'mina, V. Kuzmina, Influence sputtering conditions on electrical characteristics of Si-LiNbO3 heterostructures formed by radio-frequency magnetron sputtering, Mol. Cryst. Liq. Cryst. 603 (2014) 202–215, https://doi.org/10.1080/15421406.2014.967607.

[11] D.A. Kiselev, R.N. Zhukov, A.S. Bykov, M.I. Voronova, K.D. Shcherbachev, M.D. Malinkovich, Y.N. Parkhomenko, Effect of annealing on the structure and phase composition of thin electro-optical lithium niobate films, Inorg. Mater. 50 (2014) 419–422, https://doi.org/10.1134/S0020168514040074.

[12] H. Akazawa, M. Shimada, Mechanism for LiNb3O8 phase formation during thermal annealing of crystalline and amorphous LiNbO3 thin films, J. Mater. Res. 22 (2007) 1726–1736, https://doi.org/10.1557/JMR.2007.0208.

[13] C.S. Hwang, T. Mikolajick, Ferroelectric memories, Adv. Non-Volatile Mem. Storage Technol. (2019) 393–441, https://doi.org/10.1016/B978-0-08-102584-0.00012-7.

[14] G.H. Haertling, Ferroelectric thin films for electronic applications, J. Vac. Sci. Technol. A Vacuum, Surfaces, Film. 9 (1991) 414–420, https://doi.org/10.1116/1.577424.

[15] S. Bredikhin, S. Scharner, M. Klingler, V. Kveder, B. Red'kin, W. Weppner, Nonstoichiometry and electrocoloration due to injection of Li+ and O2− ions into lithium niobate crystals, J. Appl. Phys. 88 (2000) 5687–5694, https://doi.org/10.1063/1.1318367.

[16] S. Sanna, R. Hölscher, W.G. Schmidt, Temperature dependent LiNbO3(0 0 0 1): surface reconstruction and surface charge, Appl. Surf. Sci. 301 (2014) 70–78, https://doi.org/10.1016/J.APSUSC.2014.01.104.

[17] K.L. Sweeney, L.E. Halliburton, Oxygen vacancies in lithium niobate, Appl. Phys. Lett. 43 (1983) 336–338, https://doi.org/10.1063/1.94347.

[18] D.M. Smyth, Defects and transport in LiNbO $_3$, Ferroelectrics 50 (1983) 93–102, https://doi.org/10.1080/00150198308014437.

[19] E. Cao, Y. Zhang, H. Qin, L. Zhang, J. Hu, Vacancy-induced magnetism in ferroelectric LiNbO3 and LiTaO 3, Phys. B Condens. Matter 410 (2013) 68–73, https://doi.org/10.1016/j.physb.2012.10.030.

[20] M. Coll, J. Fontcuberta, M. Althammer, M. Bibes, H. Boschker, A. Calleja, G. Cheng, M. Cuoco, R. Dittmann, B. Dkhil, I. El Baggari, M. Fanciulli, I. Fina, E. Fortunato, C. Frontera, S. Fujita, V. Garcia, S.T.B. Goennenwein, C.-G. Granqvist, J. Grollier, R. Gross, A. Hagfeldt, G. Herranz, K. Hono, E. Houwman, M. Huijben, A. Kalaboukhov, D.J. Keeble, G. Koster, L.F. Kourkoutis, J. Levy, M. Lira-Cantu, J.L. MacManus-Driscoll, J. Mannhart, R. Martins, S. Menzel, T. Mikolajick, M. Napari, M.D. Nguyen, G. Niklasson, C. Paillard, S. Panigrahi, G. Rijnders, F. Sánchez, P. Sanchis, S. Sanna, D.G. Schlom, U. Schroeder, K.M. Shen, A. Siemon, M. Spreitzer, H. Sukegawa, R. Tamayo, J. van den Brink, N. Pryds, F.M. Granozio, Towards oxide electronics: a roadmap, Appl. Surf. Sci. 482 (2019) 1–93, https://doi.org/10.1016/J.APSUSC.2019.03.312.

[21] H. Li, Y. Xia, B. Xu, H. Guo, J. Yin, Z. Liu, Memristive behaviors of LiNbO3 ferroelectric diodes, Appl. Phys. Lett. 97 (2010), 012902, https://doi.org/10.1063/1.3462067.

[22] X. Pan, Y. Shuai, C. Wu, W. Luo, X. Sun, H. Zeng, S. Zhou, R. Böttger, X. Ou, T. Mikolajick, W. Zhang, H. Schmidt, Rectifying filamentary resistive switching in ion-exfoliated LiNbO 3 thin films, Appl. Phys. Lett. 108 (2016), 032904, https://doi.org/10.1063/1.4940372.

[23] M. Sumets, A. Kostyuchenko, V. Ievlev, S. Kannykin, V. Dybov, Influence of thermal annealing on structural properties and oxide charge of LiNbO3 films, J. Mater. Sci. Mater. Electron. 26 (2015) 7853–7859, https://doi.org/10.1007/s10854-015-3435-z.

[24] M. Sumets, V. Ievlev, A. Kostyuchenko, V. Dybov, G. Kotov, A. Sidorkin, Charge phenomena at the Si/LiNbO3 heterointerface after thermal annealing, Ceram. Int. 44 (2018) 15058–15064, https://doi.org/10.1016/J.CERAMINT.2018.05.136.

[25] S.M. Sze, K.N. Kwok, Physics of Semiconductor Devices, 3 edition, John wiley & sons, New York, 2006.

[26] A.Z. Simões, A.H.M. González, A. Ries, M.A. Zaghete, B.D. Stojanovic, J.A. Varela, Influence of thickness on crystallization and properties of LiNbO3 thin films, Mater. Char. 50 (2003) 239–244, https://doi.org/10.1016/S1044-5803(03)00089-5.

[27] M. Sumets, V. Ievlev, V. Dybov, A. Kostyuchenko, D. Serikov, S. Kannykin, G. Kotov, E. Belonogov, Electrical properties of amorphous films and crystallization of Li–Nb–O system on silicon, J. Mater. Sci. Mater. Electron. 30 (2019) 15662–15669, https://doi.org/10.1007/s10854-019-01948-z.

[28] K. Tabata, T. Choso, Y. Nagasawa, The topmost structure of annealed single crystal of LiNbO3, Surf. Sci. 408 (1998) 137–145, https://doi.org/10.1016/S0039-6028(98)00177-0.

[29] M. Deen, F. Pascal, Electrical characterization of semiconductor materials and devices, in: Springer Handb. Electron. Photonic Mater., Springer US, Boston, MA, 2006, pp. 409–438, https://doi.org/10.1007/978-0-387-29185-7_20.

[30] K. Nagai, T. Sekigawa, Y. Hayashi, Capacitance-voltage characteristics of Semiconductor-Insulator-Semiconductor (SIS) structure, Solid State Electron. 28 (1985) 789–798, https://doi.org/10.1016/0038-1101(85)90066-8.

[31] M. Kitabatake, T. Mitsuyu, K. Wasa, Structure and dielectric properties of amorphous LiNbO 3 thin films prepared by a sputtering deposition, J. Appl. Phys. 56 (1984) 1780–1784, https://doi.org/10.1063/1.334185.

[32] A.M. Glass, M.E. Lines, K. Nassau, J.W. Shiever, Anomalous dielectric behavior and reversible pyroelectricity in roller-quenched LiNbO $_3$ and LiTaO $_3$ glass, Appl. Phys. Lett. 31 (1977) 249–251, https://doi.org/10.1063/1.89670.

[33] K. Nassau, H.J. Levinstein, G.M. Loiacono, Ferroelectric lithium niobate. 2. Preparation of single domain crystals, J. Phys. Chem. Solid. 27 (1966) 989–996, https://doi.org/10.1016/0022-3697(66)90071-0.

[34] R.W. Vest, R.C.R. Wu, The electrical properties and epitaxial growth of LiNbO/sub 3/films by the MOD process, in: [Proceedings] 1990 IEEE 7th Int. Symp. Appl. Ferroelectr., IEEE, 1990, pp. 170–176, https://doi.org/10.1109/ISAF.1990.200218.